Sports Engineering (2024) 27:30
https://doi.org/10.1007/s12283-024-00474-4

ORIGINAL ARTICLE

Sticky feet: a tribological study of climbing shoe rubber

Robert J. Elkington[1] · Josh L. Armitage[1] · Thawhid Khan[2] · Michael G. Bryant[3]

Accepted: 27 August 2024

Abstract
This study examines the tribological properties of climbing shoe rubbers, challenging the common belief in the climbing community that softer rubbers are inherently grippier. This study investigates the mechanical and wear characteristics of climbing shoe rubbers by employing a high-precision modular mechanical testing environment (Bruker UMT TriboLab) and representative granite counter-surfaces. Key parameters, including surface roughness, Shore A hardness, interfacial adhesion, static and dynamic friction coefficients, and material wear patterns, were analyzed. The mechanical properties of each rubber compound were characterized through Shore A hardness testing and ball indentation–retraction tests, measuring indentation force, energy, and adhesive properties. Sliding friction tests, simulating real climbing conditions, were conducted to understand the tribological behavior of each rubber compound under different loads, further analyzing static and dynamic friction coefficients and wear characteristics. The findings of this study indicate that rubber performance is a convolution of several factors, including material hardness, surface roughness, and interfacial adhesion. Contrary to popular belief, softer rubbers did not consistently exhibit superior tribological characteristics. The findings of this study suggest that climbing shoe selection and design should consider a broader range of material characteristics beyond hardness, emphasizing the role of surface roughness and adhesion in determining overall frictional performance. This research offers valuable insights for the climbing community, providing methodologies to benchmark climbing rubber material characteristics.

Keywords Climbing · Tribology · Elastomer · Elastic mechanics

1 Introduction

Climbing shoe compounds are engineered using proprietary blends of synthetic vulcanized rubber and fillers, colloquially referred to as ‘sticky rubber’ [1]. These materials are developed for key attributes, such as abrasion resistance, flexibility, step sensitivity, slip control, and grip, in order for them to function effectively across indoor and outdoor conditions and against various rock types. Effective climbing necessitates expert manipulation of the shoe–rock interface to maximize friction in both static and dynamic situations, in addition to the climbers’ position stability.

The elastic and tribological properties of a rubber depend on its composition, including vulcanization parameters, aggregate ratios, and inorganic fillers [2]. This leads to a wide-ranging market, offering both hard and soft climbing shoe soles. Typically, harder rubbers are recommended for outdoor climbing, where resistance to plastic deformation is necessary for precise weight distribution on small and sharp features alongside dealing with steeper climbs requiring smearing against abrasive rock materials, such as granite and limestone. In contrast, softer rubbers are favored for indoor climbing, as they can deform to synthetic features and the increased surface area could impact tribological properties, thereby providing a ‘stickier’ grip [3, 4]. However, for elastomer interfaces, the impact of topography effects such as chemical adhesion or surface texturing are demonstrated to affect friction response [5], and are often overlooked by manufacturers when advertising to climbing shoe consumers.

✉ Robert J. Elkington
mnrje@leeds.ac.uk

[1] Institute of Functional Surfaces, Mechanical Engineering, University of Leeds, Yorkshire, Leeds LS2 9JT, UK

[2] Department of Mechanical Engineering, University of Sheffield, Yorkshire, Sheffield S10 2TN, UK

[3] School of Engineering, College of Engineering and Physical Sciences, University of Birmingham, West Midlands, Birmingham B15 2TT, UK

Published online: 13 September 2024

There is a broad consensus that climbing performance is enhanced most by softer rubbers—which are regarded as grippier despite the trade-off in reduced durability [4]. Conversely, kinematic analyses of competition climbing demonstrate that harder rubber soles—which support stiffness of the foot—can reduce excess energy dissipation and provide a competitive speed advantage [6]. It is therefore oversimplification to reduce climbing shoe rubber performance to solely a function of hardness. There will also be differences in adhesive and viscoelastic behavior, which in turn will impact performance, depending on the proprietary chemistry of rubber blends and the addition of fillers. There presently exists no standardized metric between climbing brands to enable a comparison of all climbing shoe rubbers.

The tribological mechanisms that define the behavior of rock-climbing interfaces can vary, based on the form of contact being involved. Movements such as 'smearing' and 'jamming' in the discipline of crack-climbing are often hypothesized to require a high and sustained static friction coefficient (μ_s), where contacting surfaces remain stationary relative to one another. The dynamic elements of rock climbing, such as foot rotation and jumping 'dyno' movements engender a dynamic friction regime as surfaces become largely in relative motion to one another. Such dynamic contacts require a higher dynamic friction coefficient (μ_d) to support the climber during relative motion with the rock [7, 8].

Undue shoe slippage can lead to eccentric stress injuries on the lower extremities, finger pulley injuries, or falling [8]. Furthermore, recent studies demonstrate excessive wear of climbing shoes can lead to inhalation of toxic rubber-derived chemicals, further necessitating standardization of testing methods of climbing rubber wear [9, 10].

This study aims to provide insights into the performance of climbing shoe rubbers within the context of materials engineering and tribology, in addition to exploring quantitative metrics for describing their behavior. Second, the near universal sentiment of 'soft rubbers are stickier' in terms of higher absolute friction—held broadly by the greater climbing community—will be addressed [11], seeking to reconcile the multifarious roles of shoe hardness, roughness, viscoelasticity, and adhesion in elastomer tribology within the context of climbing [12]. This study also serves to evaluate and discern the effects of repeated wear on both their static and dynamic friction coefficients.

There are few data on the performance of different climbing shoe rubbers and this study aims to improve on the selection, evaluation, and development of climbing shoe rubbers through the development of relevant and reproducible mechanical testing procedures. The outcomes of this research therefore contribute to the broader climbing community by offering accessible methods to benchmark climbing rubber performance.

2 Materials and methods

2.1 Material selection

Five rubber compounds were selected for analysis, owing to their prevalent use for common rock-climbing shoe outsoles. These five compounds are listed in Table 1, and are each manufactured by one of two leading climbing shoe rubber brands: Vibram (Italy) and FiveTen (Adidas, Germany). The three Vibram rubber sheets each had one surface that was textured via unidirectional scoring, as intended for use as an exterior climbing surface and an un-textured backside. Whereas the two FiveTen rubber sheets were un-textured on both faces. The textured faces of the Vibram rubber sheets were used as testing surfaces as to give an accurate representation of the climbing shoe contact interface. All rubbers were cut into 40×20 mm coupons for testing. Granite samples were obtained from the School of Civil Engineering at the University of Leeds; supplied as 10 mm diameter cylindrical pins of 20 mm length. This material coupling represents the typical material interaction present in outdoor climbing.

2.2 Shore A hardness

Shore A Hardness is a standardized method for evaluating the hardness of a material, particularly applicable to climbing shoe rubbers. As defined by ASTM D2240 [13], this procedure measures the depth of indentation created by a hardened steel rod with a beveled cylindrical tip under an applied force of 8.05 N at room temperature (22 °C). For this study, each specimen was subjected to five individual tests using a ZwickRoell Indentec Shore-A Durometer at different points on the rubber surface at room temperature (22 °C). The durometer provided an analogue read-out on a calibrated 0–100 Shore A hardness scale. The mean ± one standard deviation ($N = 5$) values for these hardness measurements were calculated and compared among the five rubber compounds.

Table 1 Rubber manufacturers and compounds used for testing

Manufacturer	Compound trade name
Vibram	XS Grip2 (XSG2) XS Edge (XSE) XS Flash (XSF)
FiveTen	Stealth Mi6 (SMi6) Stealth C4 (SC4)

2.3 Ball indentation

The mechanical characteristics of the climbing shoe rubbers were cross-validated using a custom indentation method, performed using a UMT TriboLab (Bruker, USA) (Fig. 1) to assess surface hardness and interfacial adhesion at room temperature (22 °C). A displacement-controlled indentation procedure was developed to profile the reaction force response, followed by a retraction and pull-off procedure to measure the adhesive properties of the rubber surfaces. This displacement-controlled indentation–retraction procedure involved a 12 mm diameter grade 100 AISI 52100 hardened chrome steel ball bearing, penetrating 400 µm into rubber samples at 200 μms^{-1} using a high-precision screw-driven linear actuator. Once a 400 µm indentation depth was reached, this displacement was maintained for 120 s, allowing for viscoelastic stress relaxation to occur within the strained rubber. The ball bearing was then retracted from the rubber sample at 1 μms^{-1} to evaluate contact adhesion.

The steel bearings are consistent counter-surfaces of a known hardness suitably higher than that of the rubbers being tested. The thickness of these rubber samples ranged from 3.5 to 4.2 mm. Despite the indentation depth for this procedure being ~ 10% of the sample thickness, the exact magnitude of indentation remained absolute to represent consistent conditions. The rubber samples were fixed to a stationary polished stainless-steel substrate with cyanoacrylate adhesive, reducing sample migration.

The relatively high speed of indentation allowed for deformation to occur on a timescale significantly shorter than the expected timescales for viscoelastic creep deformation [14]. Therefore, a greater proportion of the material response during this phase is elastic as opposed to viscous, representing the expected material response during climbing. The peak normal reaction force at 400 µm during indentation (F_{ind}) was recorded for each rubber by a DFH-5G (Bruker, USA) strain gauge load cell with 25 mN precision. The total indentation energy (E_{ind}) was also calculated by integrating the normal reaction force (F_z) as a function of indentation depth (z) as per Eq. (1) [15].

$$E_{ind} = \int_{0}^{400\mu m} F_z(z)dz \tag{1}$$

During the retraction phase of this procedure, a negative normal reaction force implies that adhesive forces are holding the ball and rubber surface together as the ball is 'pulling off' from the contact. The minimum value of this force is the peak pull-off force (F_{adh}), and the total adhesion energy (E_{adh}) is calculated as per Eq. (2).

$$E_{adh} = \int_{400\mu m}^{-200\mu m} F_z\left(F_z < 0\right)dz \tag{2}$$

2.4 Sliding friction

A repeat wear sliding friction assessment was performed using a Bruker UMT TriboLab to ascertain the tribological properties of each rubber under simulated climbing conditions. The testing regime is summarized in Table 2, with the test apparatus depicted in Fig. 2.

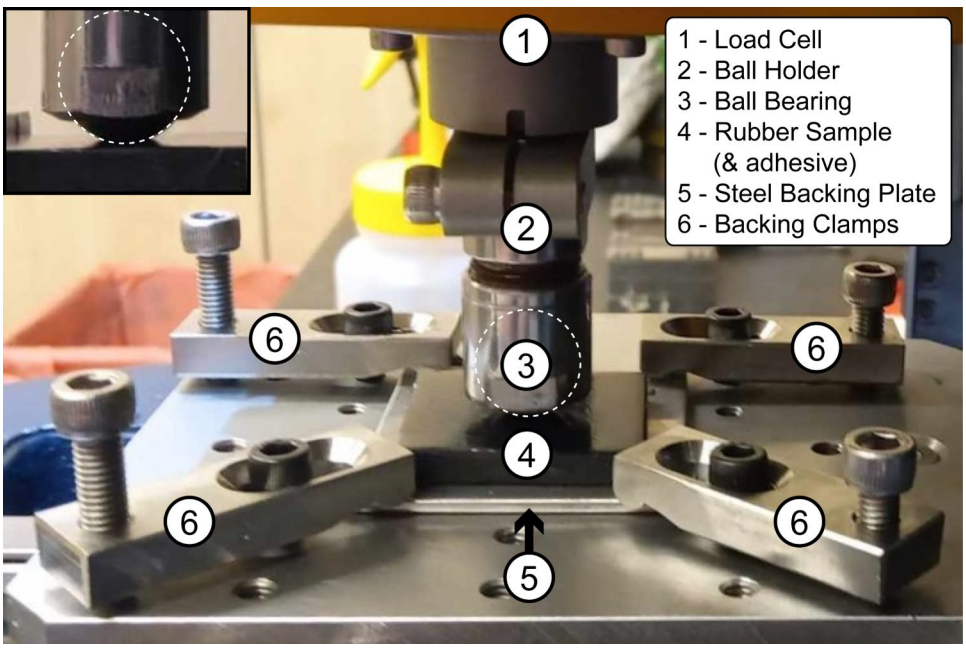

Fig. 1 Schematic of the UMT TriboLab configuration for indentation tests demonstrating the bearing–rubber interface

Table 2 Tribological testing parameters for the repeat wear testing regime

Contact	Sliding test parameters	Rubber compounds
Granite Pin on Rubber Plate	F_z = 30 / 60 N (P = 0.38 / 0.76 MPa)	XSG2
	v = 0.1 mm/s	XSF
	Δx = 10 mm	XSE
	N = 5	SMi6
		SC4

For each sliding test, the circular face of the cylindrical granite pin was initially brought into contact with the rubber counter-surface and indented using a high-precision screw-driven linear actuator until the given normal reaction force was reached. Once this normal force was reached, the pin was then slid laterally across the rubber surface using a second linear actuator. The pin was slid laterally by 10 mm at a speed of 0.1 mm/s for all tests. Indentation experiments were conducted under a normal load (F_z) of 30 N and 60 N, corresponding to a contact pressure of 0.38 MPa and 0.76 MPa respectively. This loading corresponds to a rough estimation that for a 75 kg climber a total of 10–20 cm^2 nominal shoe area is in contact during climbing, corresponding to a contact pressure of 0.37–0.74 MPa.

These test parameters were carried out twice for each rubber compound, with the first iteration being utilized as an initial 'wearing-in' stage where no data was collected. This 'wear-in' procedure allows for a more realistic representation of the shoe rubbers in a typical climbing scenario. Utilizing this testing regime, five (N = 5) consecutive repeat tests were performed on each rubber compound, with twenty-five (N = 25) tests in total being carried out.

A proportional-integral-derivative (PID) control system was implemented to precisely adjust vertical displacement and maintain a constant normal force across the sliding motion. A DFH-5G (Bruker, USA) strain gauge load cell was implemented to measure both normal and tangential forces at 100 Hz. The ratio of the tangential force (F_x) to normal force is commonly referred to as the friction coefficient (μ) in tribological analyses, as shown in Eq. (3). The encoders for both actuators concurrently recorded sliding displacement (Δx) along with the time-dependent friction coefficient ($\mu(t)$).

$$\mu(t) = \frac{F_x(t)}{F_z(t)} \tag{3}$$

In order to better illustrate the overall tribological performance of these rubbers during the transition between static and dynamic friction behaviors, the term 'slip factor' (κ) is introduced. κ is defined as a measure of how drastic this transition is for a given interface using Eq. (4).

$$\kappa = 1 - \frac{\mu_d}{\mu_s} \tag{4}$$

An interface with a higher slip factor indicates that its friction coefficient would be reduced by a larger degree upon the transition from stick regime to slip regime. The static friction coefficient (stick regime, μ_s) for a given test was determined as the height of the initial high-friction peak for each test (the earliest point at which $d\mu(t)/dt = 0$), and the dynamic friction coefficient (slip regime, μ_d) was determined as the second local minima in $\mu(t)$, after the point where μ_s is determined, as highlighted in Fig. 9. The determination of dynamic friction as the second minima (where $d\mu(t)/dt = 0$) is to avoid the contribution of shear stresses attributed to rubber pinching (i.e., physical obstruction) during sliding.

2.5 Surface topography and wear

An NPFLEX (Bruker, USA) optical interferometer was used to generate three-dimensional surface heightmaps for each rubber using a non-contact vertical scanning interferometry (VSI) method at 20× optical magnification. Three separate

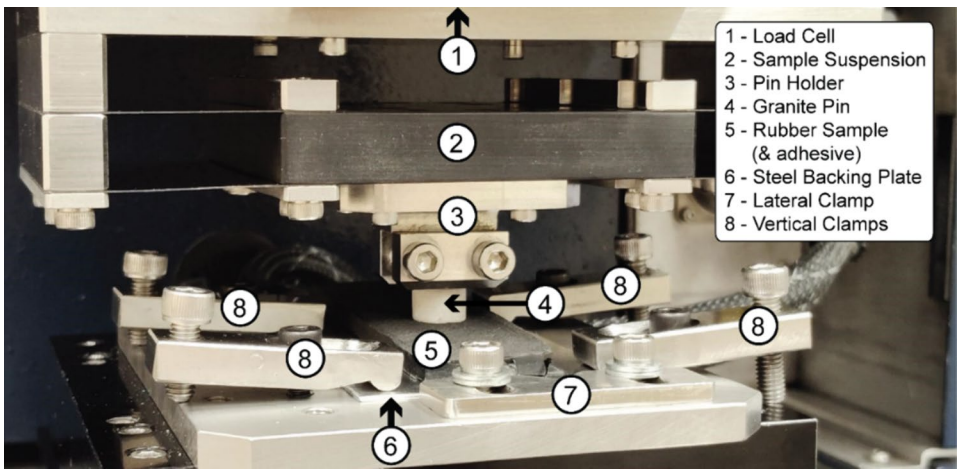

Fig. 2 Schematic of the UMT TriboLab configuration for sliding friction tests, demonstrating the granite pin–rubber interface

2 × 2 mm areas of each surface were scanned ($N = 5$). A high intensity monochromatic green light source was used to generate sufficient reflections from the comparatively non-reflective rubber surfaces. Each heightmap was processed using Vision64 (Bruker, USA) software in conjunction with a bespoke MATLAB script to calculate the arithmetic mean roughness (R_a) of each surface.

This VSI method was also utilized to measure the volume loss and wear depth of the rubber compounds after the tribometer tests. However, it was not possible to measure the wear depth and volume loss after testing due to the negligible material loss of each compound. The contact area for each sample was examined using an optical microscope (Leica DM6000 M), allowing for the wear scar length and width to be measured by visual inspection. The microscope was also utilized to capture any visual changes to the surface appearance and topography post-testing.

2.6 Statistical analysis

In this study, both Pearson and Spearman correlation analyses were employed to evaluate the relationships between the static and dynamic friction coefficients of climbing shoe rubbers and various material properties, including Shore A hardness, surface roughness (R_a), indentation force (F_{ind}), indentation energy (E_{ind}), adhesive force (F_{adh}), and adhesive energy (E_{adh}). The Pearson correlation coefficient measures the strength and direction of the linear relationship between two variables. It is calculated by dividing the covariance of two variables by the product of their standard deviations. The Spearman rank correlation coefficient (ρ) assesses the strength and direction of the monotonic relationship between two ranked variables. Unlike Pearson, Spearman does not assume that the relationship between the variables is linear and is therefore less sensitive to outliers. Both Pearson and Spearman coefficients range from −1 to 1, where 1 indicates a perfect positive correlation, −1 indicates a perfect negative correlation, and 0 indicates no relationship.

3 Results

3.1 Surface topography

Figure 3 shows example greyscale images of surface height for VSI scans of each surface. The prominent rough unidirectional texturing of the XSG2, XSE, and XSF sample surfaces is highlighted in comparison with the smoother SC4, SMi6 sample surfaces. Table 3 summarizes the arithmetic mean-plane roughness (R_a) of the five different rubber compounds and their respective standard deviations. XSF exhibited the highest arithmetic mean-plane roughness ($R_a = 22.88 \pm 1.5\ \mu m$), followed by XSG2 and XSE. Comparatively, SC4 and SMi6 exhibited the lowest R_a values, with SC4 possessing the smoothest surface ($R_a = 1.77 \pm 0.2\ \mu m$).

3.2 Shore A hardness

Table 4 summarizes the mean Shore A Hardness and standard deviation for each rubber compound sample. Among the examined compounds, the SC4 rubber exhibited the highest mean hardness rating of 75 ± 0.00, whilst SMi6 had the lowest of 60.6 ± 0.45.

3.3 Ball indentation

Figure 4 depicts the mean normal reaction force (F_z) and respective standard deviation over indentation depth (z) for a series of three identical indentation tests against each rubber compound sample. The SMi6 rubber exerted the lowest reaction force of 12.9 N upon reaching 400 µm indentation depth, whereas the SC4 rubber yielded the highest of 31.4 N. These forces are proportionally consistent with the Shore A hardness values for these two rubbers. XSE also remains the second hardest rubber with the second highest indentation force, whilst XSG2 and XSF once again were consistent with their respective Shore A hardness ratings. The Shore A hardness values are also found to be commensurate with the calculated values of total indentation energy, with SMi6 and SC4 requiring the lowest and highest energies to indent at 2.39 mJ and 5.86 mJ respectively. The normal reaction force is shown to rise in a non-linear fashion as a function of indentation depth during the indentation procedure of each rubber compound. This is most notably observed during the first 200 µm of indentation, and is most prominently exhibited by the textured XSG2, XSE, and XSF rubbers surfaces.

Figure 5 depicts the normal reaction force over retraction displacement during the pull-off phase of indentation testing. The peak pull-off force and adhesion energy for each rubber compound is summarized in Table 5. The highest adhesion energies were observed for the SMi6 and SC4 rubbers, which were measured to be approximately an order of magnitude higher than those of their textured Vibram counterparts. The adhesion energies of the FiveTen rubbers were also shown to have a substantially larger margin of error regarding repeatability, which implies that external factors such as surface contamination and humidity may have a larger influence on the adhesion of these more conformal interfaces.

3.4 Sliding friction

The friction behavior of each rock-climbing shoe outsole rubber composition is depicted in Fig. 6a, b for under the 30 N and 60 N loading scenarios respectively. The friction

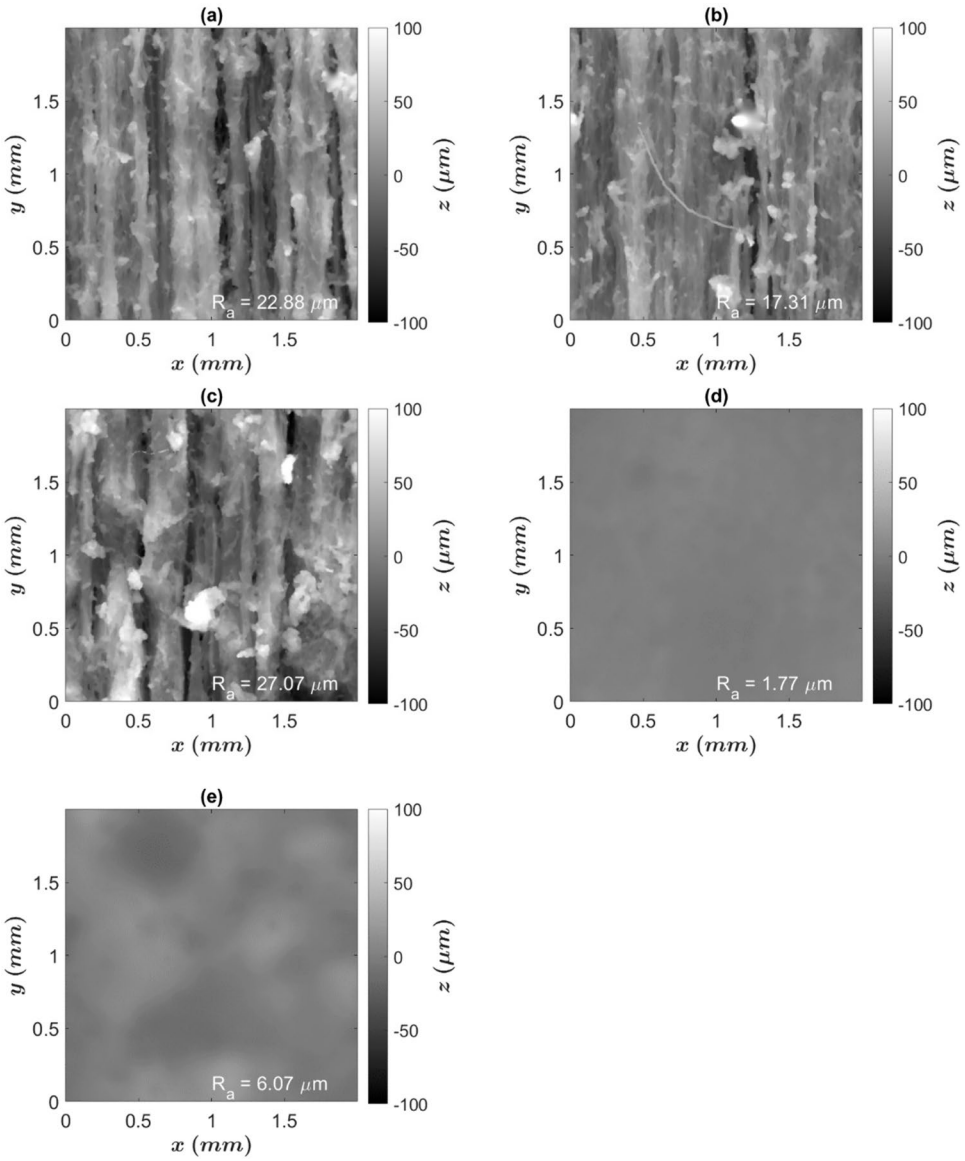

Fig. 3 Example height maps of the **a** XSG2, **b** XSE, **c** XSF, **d** SC4 and **e** SMi6 rubber surfaces, attained through green-light vertical scanning interferometry

Table 3 Mean arithmetic mean-plane roughness (R_a) and respective standard deviation ($N=3$) for each rubber compound

Rubber compound	R_a(μm)
XSG2	22.88 ± 1.5
XSE	17.31 ± 0.8
XSF	27.07 ± 1.8
SC4	1.77 ± 0.2
SMi6	6.07 ± 0.3

Table 4 Mean Shore A hardness and respective standard deviation ($N=5$) for each rubber compound

Rubber compound	Mean hardness ($N=5$)
XSG2	69.6 ± 0.45
XSE	74.2 ± 0.37
XSF	69.2 ± 0.68
SC4	75 ± 0.00
SMi6	60.6 ± 0.45

response from each rubber compound exhibits an initial 'stick' phase—characterized by an initial peak in friction coefficient occurring within the first 7–35 s of lateral motion—followed by a transition to more dynamic sliding with increasing lateral displacement.

Similar friction trends are observed under both loading scenarios, with the SMi6 rubber exhibiting the highest overall friction response in magnitude, and XSF exhibiting the lowest. An increase in friction coefficient is observed at higher displacements for most sliding tests, which is more prominent under a normal load of 60 N.

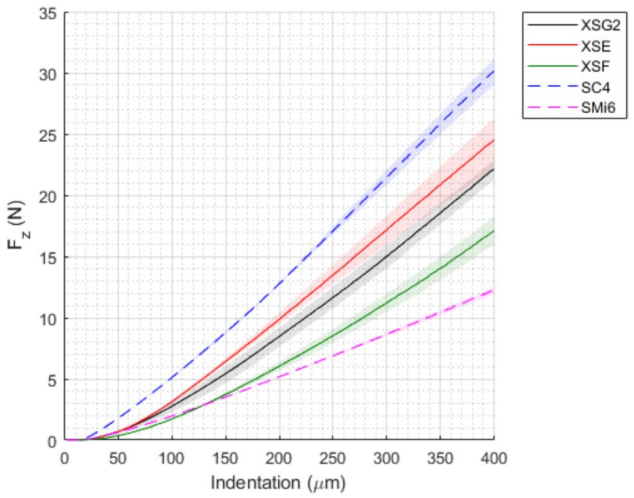

Fig. 4 Measured normal reaction force (F_z) response as a function of indentation depth (x) for each rubber compound ($N=3$) during the loading phase of the ball indentation procedure

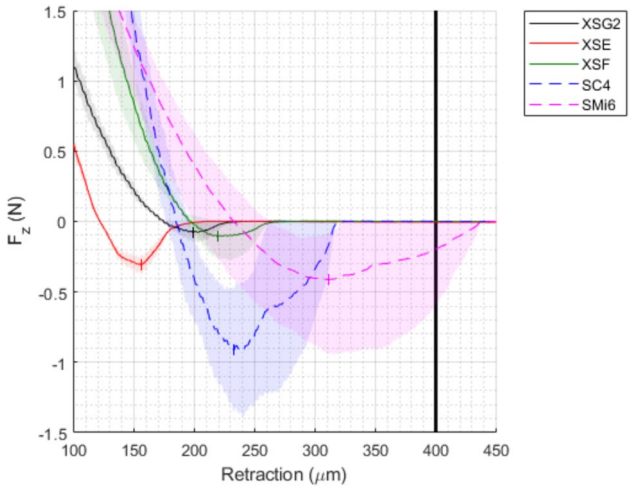

Fig. 5 Measured normal reaction force (F_z) response as a function of retraction displacement for each rubber compound during the retraction phase of the ball indentation procedure. The bold vertical line indicates the original unperturbed surface height

Table 5 Summary of the maximum indentation force and energy (F_{ind}, E_{ind} respectively) at the end of the indentation and maximum pull of force and energy (F_{adh}, E_{adh}) during the indenter retraction phase for the ball Indentation regime

Rubber	R_a(μm)	F_{ind}(N)	E_{ind}(mJ)	F_{adh}(N)	E_{adh}(μJ)
XSG2	22.9 ± 1.4	23.2 ± 0.8	4.04 ± 0.23	0.09 ± 0.04	2.82 ± 2.25
XSE	17.3 ± 1.2	25.3 ± 1.6	4.44 ± 0.35	0.31 ± 0.05	12.8 ± 3.20
XSF	27.1 ± 1.9	20.9 ± 1.1	3.18 ± 0.15	0.11 ± 0.15	4.69 ± 4.53
SC4	1.77 ± 0.2	31.4 ± 1.0	5.86 ± 0.10	0.92 ± 0.40	72.8 ± 54.3
SMi6	6.07 ± 0.4	12.9 ± 0.2	2.39 ± 0.04	0.42 ± 0.4	52.7 ± 47.8

Figure 7 compares the static and dynamic friction coefficients for each rubber composition under both loading scenarios. The SMi6 rubber yields the highest static friction coefficient under both loading scenarios, with SC4 having the second highest under 30 N but the lowest under 60 N. The XSG2 compound exhibits a higher static friction coefficient than the XSE and XSF compounds, with XSF exhibiting the lowest overall. The SMi6 rubber exhibits the highest dynamic friction under the 30 N loading scenario, followed by the SC4 and XSG2, XSE, and XSF compounds respectively. These trends remain consistent in the 60 N loading scenario, however the dynamic friction of the XSG2 and SC4 rubbers exhibit almost identical values.

The slip factor (κ) for each rubber compound and under each loading scenario is listed in Table 6, alongside their respective static and dynamic friction coefficients. The SMi6 and SC4 rubbers consistently exhibit the lowest slip factors under both 30 N and 60 N loading scenarios, with SMi6 exhibiting a slip factor as low as 1.7% under an applied load of 30 N. All rubbers exhibit a higher slip factor under 60 N of applied load than under 30 N, indicating that a higher applied load induces a more drastic friction transition upon the onset of slip.

3.5 Material wear

Figure 8 compares the wear scar dimensions of the post-tested rubber compounds under both loading scenarios. The SMi6 and XSG2 compounds exhibited the largest wear scar dimensions under the 30 N loading scenario, with the SC4 compound closely following. The XSE compound exhibited less overall wear than the SMi6, XSG2, and SC4 compounds, with the XSF surfaces also exhibiting barely visible wear patterns. Similar trends were observed under the higher 60 N loading scenario, with the SMi6 compound exhibiting the highest overall wear and the XSF the lowest. The high wear trends observed with the SMi6 compound are attributed to its low hardness. The anomalously low wear trends observed with the XSF compound may similarly be attributed as a combination of its low hardness and high surface roughness, allowing asperities to deform more easily without fracture and removal.

Differences in wear scar dimensions are observed between the two different loading scenarios. Shorter wear scars are seen for all compounds under 60 N loading, which is attributed to a higher degree of surface 'pinching' ahead of the sliding contact, evidence of which is highlighted in Fig. 9 as elevated ridges running horizontally to the sliding direction at the end of each wear scar. Figure 9 depicts example wear scars of each compound under the 30 and 60 N loading scenarios. The wear scars present on the SMi6 compound surfaces all exhibit a similarly smooth topography, with increased signs of adhesion and ploughing that

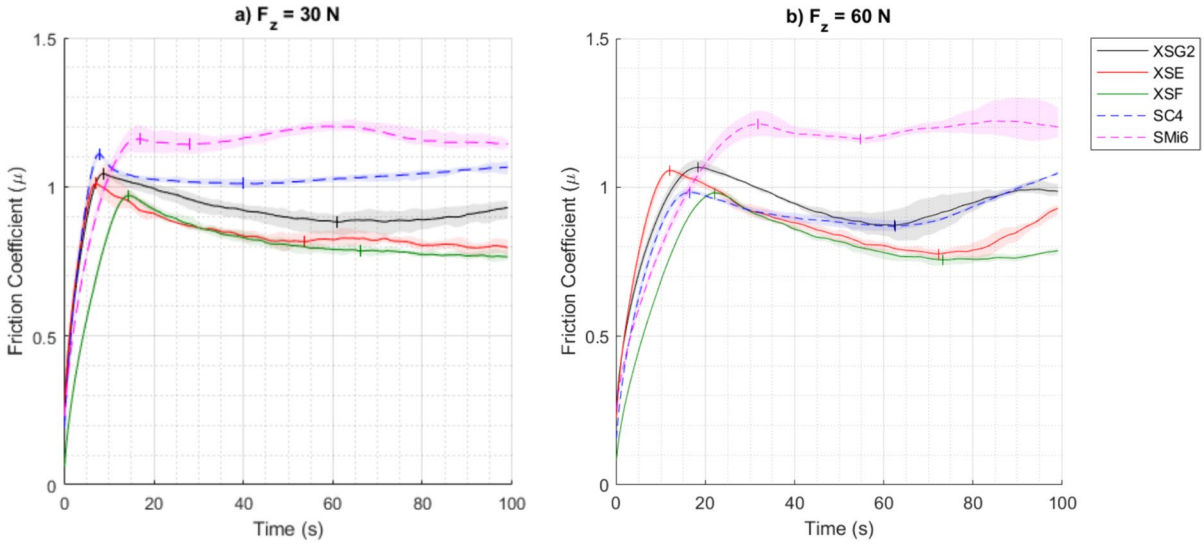

Fig. 6 Friction coefficient (μ) against time for all compared brands under a normal load of **a** 30 N and **b** 60 N; highlighting the points where static and dynamic friction coefficients (μ_s, μ_d) are noted with vertical dashes, and one standard deviation ($N=5$) denoted by shaded overlays

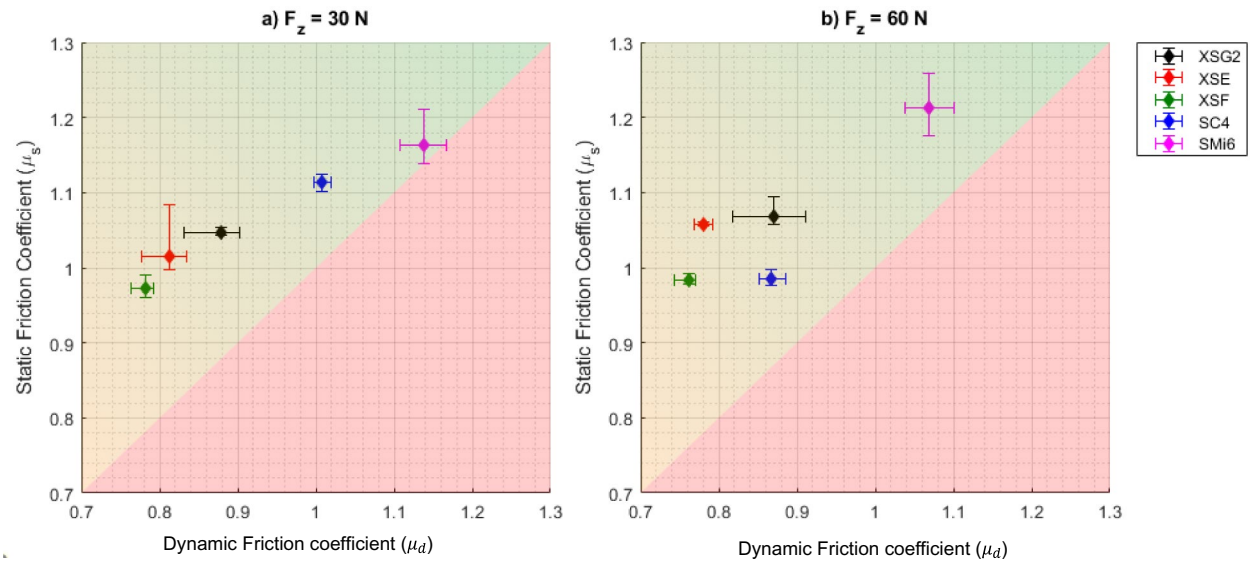

Fig. 7 Dynamic friction coefficient (μ_d) against static friction coefficient (μ_s) for all compared brands under a normal load of **a** 30 N and **b** 60 N. Standard deviation ($N=5$) is denoted by the error bars

Table 6 Highlights the static and dynamic friction coefficient (μ_s, μ_d) with standard deviation, and Slip factor (κ) under loads of 30 and 60 N

Rubber	μ_s (30 N)	μ_k (30 N)	μ_s (60 N)	μ_k (60 N)	κ (30 N) (%)	κ (60 N) (%)
XSG2	1.05 ± 0.01	0.88 ± 0.05	1.07 ± 0.05	0.87 ± 0.03	16.2	18.7
XSE	1.01 ± 0.07	0.81 ± 0.04	1.06 ± 0.01	0.78 ± 0.01	19.8	26.4
XSF	0.97 ± 0.03	0.78 ± 0.02	0.98 ± 0.01	0.76 ± 0.02	19.6	22.4
SC4	1.11 ± 0.01	1.01 ± 0.01	0.98 ± 0.01	0.87 ± 0.02	9.0	11.2
SMi6	1.16 ± 0.05	1.14 ± 0.04	1.21 ± 0.05	1.07 ± 0.03	1.7	11.6

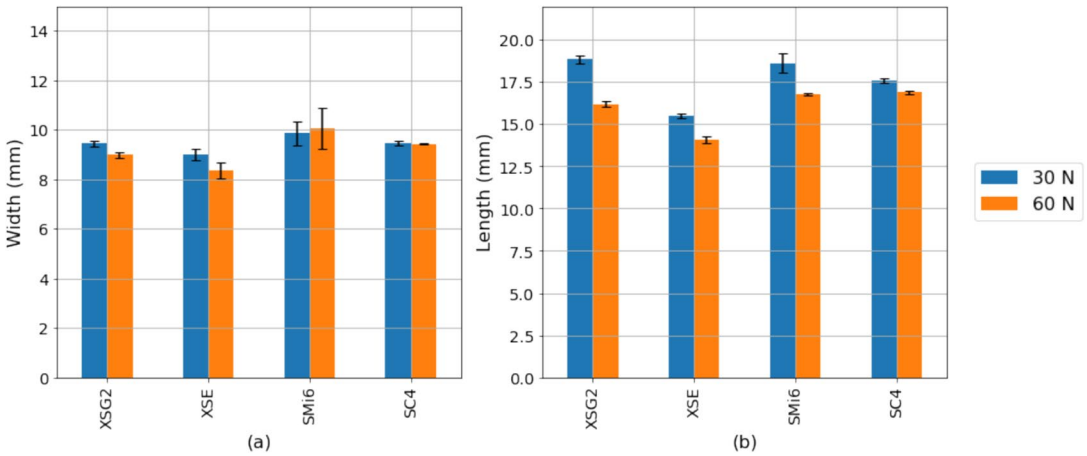

Fig. 8 Mean wear scar width **a** and length **b** of post-tests rubber samples under 30 N (blue) and 60 N (orange), examined via optical microscope. Error bars denote one standard deviation ($N=5$) for each dataset. The XSF compound dimensions is omitted from the graph due to high uncertainty quantifying wear scar dimensions

indicate the removal of material during sliding. The wear scars present on the SC4 compound surfaces exhibit an increased roughness, with prominent signs of abrasive wear in the form of unidirectional scoring and ploughing. The textured XSG2, XSE, and XSF compound surfaces all retained aspects of their unperturbed textures post-testing. The wear-scar topographies of the post-worn XSG2 and XSE surfaces indicate a truncation of their profiles, indicating the removal of asperity peaks during sliding. The XSF surfaces exhibited negligible changes to surface topography as a result of sliding tests.

4 Statistical analysis

Pearson (P) correlation coefficients and Spearman's (S) rank correlation were used to analyse both the linear and non-linear monotonic relationship between static friction coefficient (μ_s) and dynamic friction coefficient (μ_d) for 30 N and 60 N tests against Shore A hardness, surface roughness (R_a), indentation force (F_{ind}), indentation energy (E_{ind}), adhesive force (F_{adh}), and adhesive energy (E_{adh}) in Table 7.

Analysis of the lower 30 N load static friction coefficient demonstrates a strong negative correlation with rubber roughness (R_a, $P=-0.86$, $S=-0.80$) and substantial positive correlation with adhesive energy (E_{adh}, $P=0.81$, $S=0.60$). Conversely for static friction at the higher 60 N load a weak negative correlation is observed for surface roughness (R_a, $P=-0.29$, $S=-0.10$) and weak correlation for adhesion energy ($E_{adh,}$ $P=0.15$, $S=-0.15$). Instead, static friction coefficient for the higher 60 N load exhibits a negative correlation with hardness (Shore A, $P=-0.81$, $S=-0.56$) and subsequently a strong negative correlation with indentation force (F_{ind}, $P=-0.79$, $S=-0.56$).

For the dynamic friction coefficient, both the 30 N and 60 N test conditions demonstrated a consistent negative dependence on surface roughness R_a (30 N, $P=-0.84$, $S=-0.80$ and 60 N, $P=-0.63$, $S=-0.67$) and a strong positive correlation with E_{adh} for the 30 N test ($P=0.81$, $S=0.60$) and a moderate positive correlation with E_{adh} for the 60 N load ($P=0.57$, $S=0.41$). Dynamic conditions only exhibit a moderate negative linear dependence on Shore A hardness with markedly higher Pearson coefficients compared to Spearman (30 N, $P=-0.57$, $S=-0.10$ and 60 N $P=-0.77$, $S=-0.21$).

5 Discussion

The interplay between rubber composition and performance underpins the climber's ability to maintain grip and control. The following discussion elucidates this nuanced relationship between material properties, adhesive capabilities, and friction performance of climbing shoe rubbers, drawing on quantitative analyses to address conventional consumer perceptions in the sport. This discussion delves beyond surface-level interpretations, offering a comprehensive understanding of how climbing shoe rubbers behave under varying conditions, thereby informing design, selection, and application strategies for optimal climbing performance.

5.1 Material properties

The values of the Shore A hardness results obtained in this study (Table 4) correlate with those stated in the Vibram repair catalogue for the XSG2, XSE and XSF rubbers as highlighted in Table 8 [3] despite being comparatively lower by a small degree.

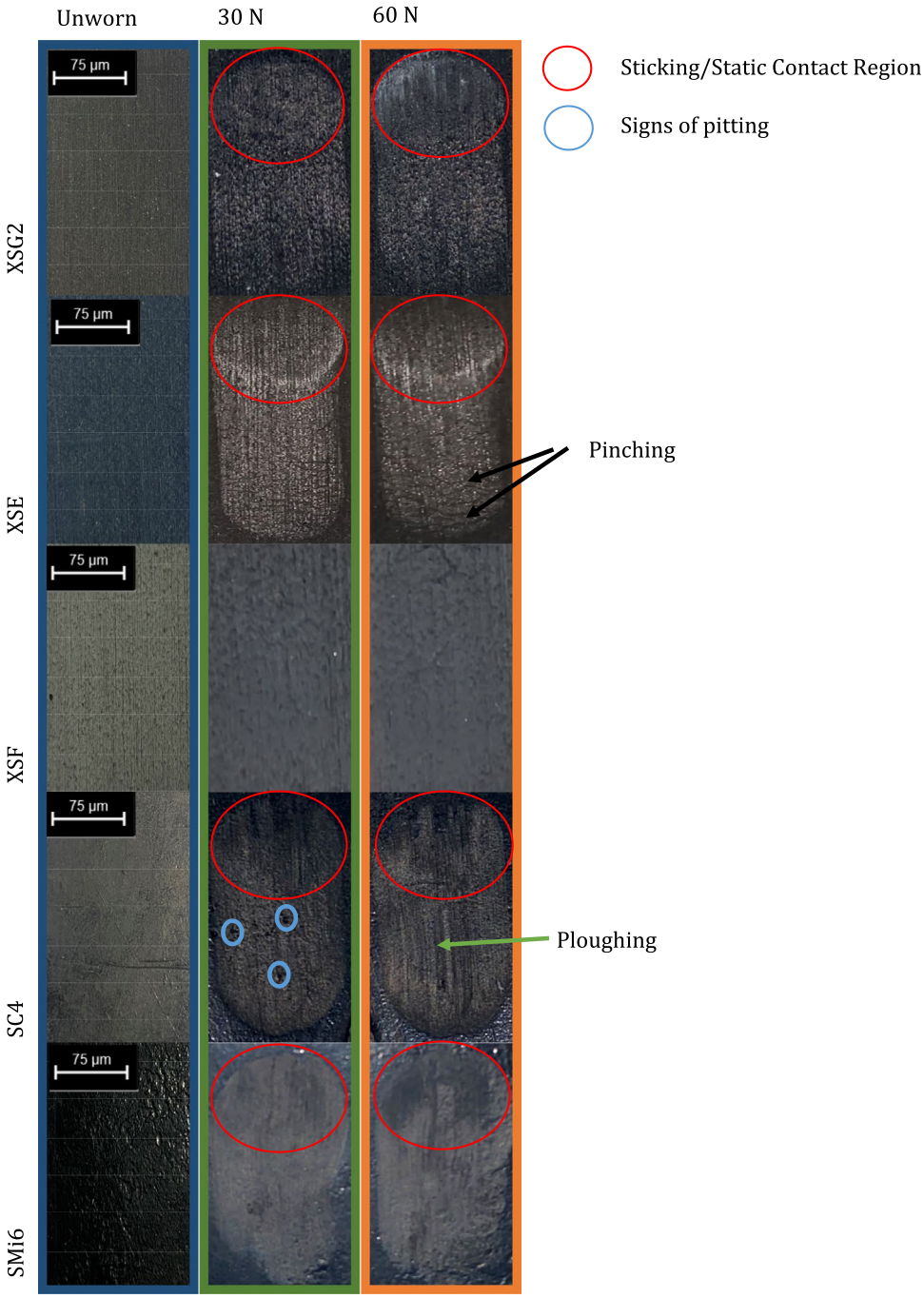

Fig. 9 Images of the unworn and worn surfaces (30 N and 60 N) of the five rubber samples showing areas of sticking, signs of pitting, and ploughing. Sliding direction is down the page

Table 7 Pearson (P) and Spearman (S) analysis of the relationship between static friction coefficient (μ_s) and dynamic Friction coefficient (μ_d) for 30 N and 60 N tests against Shore A hardness, surface roughness (R_a), indentation force (F_{ind}), indentation energy (E_{ind}), adhesive force (F_{adh}), and adhesive energy (E_{adh})

Test		Shore A	R_a	F_{ind}	E_{ind}	F_{adh}	E_{adh}
30 N Static (μ_s)	Pearson	−0.47	−0.86	−0.25	−0.04	0.60	0.81
	Spearman	−0.10	−0.80	−0.10	−0.10	0.60	0.60
30 N Dynamic (μ_d)	Pearson	−0.57	−0.84	−0.35	−0.15	0.57	0.81
	Spearman	−0.10	−0.80	−0.10	−0.10	0.60	0.60
60 N Static (μ_s)	Pearson	−0.81	−0.29	−0.79	−0.66	−0.15	0.15
	Spearman	−0.56	−0.10	−0.56	−0.56	−0.15	−0.15
60 N Dynamic (μ_d)	Pearson	−0.77	−0.63	−0.60	−0.42	0.27	0.57
	Spearman	−0.21	−0.67	−0.21	−0.21	0.41	0.41

Table 8 Shore A hardness values as measured and quoted from the Vibram repair catalogue regarding the Vibram rubber compounds [3]

Vibram rubber compound	Measured mean hardness	Catalogue hardness value
XSG2	69.6 ± 0.45	74 ± 3
XSE	74.2 ± 0.37	78 ± 3
XSF	69.2 ± 0.68	70 ± 3

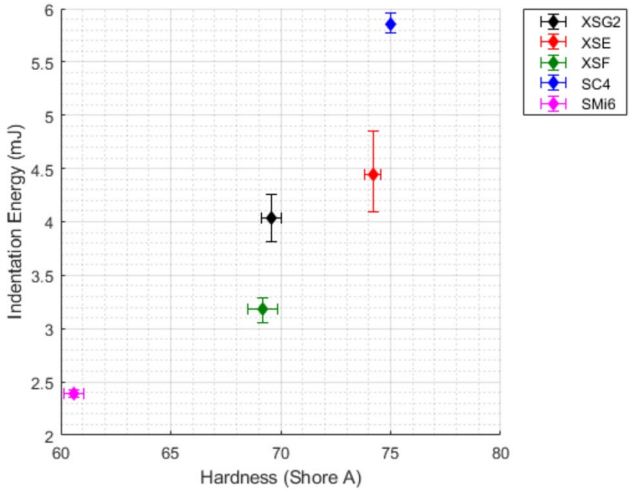

Fig. 10 Integrated indentation energy (E_{ind}) against Shore A hardness for all rubber compounds. Standard deviation ($N = 5$ for Shore A, $N = 3$ for Ball-Indentation) is denoted by the error bars

Indentation force and energy are shown to be consistent with Shore A hardness measurements as shown in Fig. 10. The caveat to this is that the XSG2, XSE and XSF compounds exhibit lower indentation energy values than what may be expected from a linear relationship between F_{ind} and E_{ind} (Fig. 10). This is caused by the exaggerated non-linear nature of how indentation force rises with indentation displacement for the textured XSG2, XSE, and XSF compounds (Fig. 4). Setting aside any time-dependent viscoelastic effects, this non-linearity may be attributed to the higher surface roughness parameters of the textured XSG2, XSE, and XSF rubbers opposed to their SMi6 and SC4 rubber counterparts, explained by prominent surface asperities deforming more easily against the spherical geometry of the bearing indenter ahead of bulk rubber deformation [16]. It has been shown that asperities of smoother surfaces generally exhibit less deformability in contact interactions compared to those of rougher surfaces [17]. This may show textured surfaces as being softer than their un-textured counterparts when elastic moduli and Poisson's ratios of the compared materials are identical.

This artefact may not be reflected as prominently in the Shore A hardness measurements due to two primary factors. First, Shore A hardness testing measures a material's resistance to plastic deformation. Therefore, the observed contact pressures during hardness testing are substantially higher than what is observed for the ball indentation tests as to measure the elastic limit of a material. Secondly, the geometry of the Shore A indenter is smaller than the expected contact area for the ball indentation tests. Not only does this attribute to the higher observed contact pressures for hardness testing, but it also implies that the indentation procedure involving a 12 mm radius polished steel ball is more sensitive to the surface topography of the rubber samples than the more localized hardness tests.

This difference in contact area is reflected in the hardness and ball indentation data, implying that the Shore A hardness results are a more localized reflection of bulk material properties, therefore less sensitive to surface topography and asperity deformation than the ball indentation tests. It was shown that despite the similar Shore A hardness of the XSE (Shore A = 74.2) and SC4 (Shore A = 75) samples the difference in indentation energy was more pronounced when considering the effect of roughness of the XSE ($E_{ind} = 4.44$ mJ) compared to the smoother SC4 ($E_{ind} = 5.86$ mJ).

Upon comparing the findings in Tables 4 and 5, it is apparent that the adhesive capabilities of each rubber surface is independent of material hardness. The highest adhesive energies and peak pull-off forces were instead observed for the softest (SMi6) and the hardest (SC4) rubbers respectively. SMi6 and SC4 do both exhibit low arithmetic mean plane surface roughness's (R_a) of 6.07 µm and 1.77 µm respectively, whereas the Vibram samples have R_a values ranging between 17.3–27.1 µm.

This indicates that while adhesion is strongly affected by the specific surface chemistries of each rubber compound [18], the adhesion energy may be primarily dominated by surface roughness when comparing these contacts [19]. The smoother FiveTen rubber surfaces achieved a higher degree of contact conformity, and subsequently a greater real contact area, during the ball indentation tests. Conversely, the asperities of the rougher Vibram rubbers may not have fully conformed to the topography of the smooth steel countersurface, giving rise to a spatially discontinuous real area of contact [20]. A notable observation in our study is the substantial adhesion strength between the ball and the SMi6 surface. This adhesion is strong enough to elevate the rubber surface 35 µm above its initial height before the loss of contact during retraction. In contrast, the point of separation remained below the original surface height for all other rubber compounds.

5.2 Sliding friction

All sliding friction tests exhibit an initial 'stick' phase. This transition represents stick–slip behavior and the transition

from static (μ_s) to dynamic (μ_d) friction, indicating that there exists a critical shear value that must be exceeded for the contact to initial lateral slipping [21]. The low moduli of rubbers also imply that there may be separate regions within the real contact area which may be experiencing stick and slip simultaneously [22].

A rise in $\mu(t)$ is often seen towards the end of the sliding displacement for the 60 N tests. This rise is caused by the buckling and pinching of the rubber surface ahead of the granite pin as it travels, which is most notably observed under a load of 60 N (Fig. 6b). Evidence of this phenomenon can be observed in Fig. 9, where images of the edge wear track at 60 N pinching can be observed [23]. There is only one test series which does not exhibit this behavior, and that is for the XSF rubber under a load of 30 N. No signs of pinching were observed on this sample as depicted in Fig. 9, which indicates that pinching of the rubber surface ahead of the contact may directly influence the perceived friction coefficient at higher displacements owing to physical obstruction of the sliding pin.

Several key trends within existing literature are identified and corroborated in this study, including the findings of Voigt et al. [18] which analyzed the friction, adhesion, and wear characteristics of 18 synthetic polymeric rubber materials. The transitions from stick to slip regime observed in the lateral friction tests of this study are consistent with the stick–slip behavior reported by Voigt et al. [18] sliding tests. The presented data also reveal that the onset of the transition from stick to slip friction regime occurs at a significantly later displacement for the softest SMi6 and XSF samples in comparison to the harder XSG2, SC4, and XSE compounds under both applied loading conditions. Moreover, the stick regime endures longer for all tested rubber compounds under the higher 60 N loading scenario (Fig. 9). These prolonged stick phases suggest that the softer rubber samples are able to deform and sustain tangential shear across their bulk to a larger extent of lateral surface displacement before initiating interfacial slip across the majority of the real contact area [17].

The static friction coefficient is a measure of the maximum shear stress within the contact before the onset of slip regime sliding behavior, relative to the applied normal force. Therefore, the friction response for the initial stick phase of each test can be viewed as an interfacial tangential equivalent of a traditional tensile strength test, and the rate at which the measured tangential force rises with lateral displacement may give a measurement for the effective shear moduli of the interface. This relationship can clearly be seen upon comparison of the two softest rubbers, SMi6 and XSF, showing a slower increase in friction coefficient over lateral displacement.

Existing literature demonstrates that softer rubbers generally exhibit higher friction coefficients, as observed by Heinrich et al. [18, 24]. The SC4 and XSF surfaces are inconsistent with these expected behaviors; with SC4 being the hardest rubber and exhibiting the second highest friction coefficients under 30 N, and XSF being the second softest rubber exhibiting the lowest friction coefficients under both loading scenarios. The SC4 compound exhibited a markedly higher adhesion energy ($E_{adh} = 72.8$ mJ) than the XSE compound ($E_{adh} = 12.8$ mJ) despite their similar Shore A hardness. This difference in adhesion energy is instead attributed to differences in surface chemical composition, in addition to the higher surface roughness of the XSE rubber. Furthermore, the XSF rubber exhibits the second lowest hardness and surface adhesion energy, alongside having the highest surface roughness. All of these factors are likely to contribute to its overall friction behavior being least favorable.

It is evident from these findings that the two rubbers with the highest adhesion energy, SMi6 and SC4, also exhibit the highest static and dynamic friction coefficients under a load of 30 N. Similar trends were observed by Voigt et al. [18] and other studies [25, 26] where softer and more adhering surfaces led to higher static and dynamic friction coefficients for a diverse range of industrial shoe rubber samples. Their findings show that a decrease in friction behavior was observed with increased rubber hardness [27]. These findings therefore do not consistently scale with hardness alone. Instead, friction performance is evidently a convolution of rubber hardness and contact topography, along with surfaces chemical composition and resulting adhesive effects.

Analysis of the statistical correlation data reveals key insights into the role of rubber surface and mechanical parameters under static and dynamic conditions (Table 7). For a climber, the most pertinent metric would be the rubber behavior under static conditions, realizing that performance climbers optimize footwork to move in a controlled way to avoid instabilities caused by 'stepping off' a climbing shoe during slip [11]. The strong negative correlation between static friction coefficient (μ_s) and surface roughness (R_a) at lower loads (30 N) suggests that as the surface roughness increases, the rubber's compliance with the contact area decreases, leading to a reduction in friction. This behavior is expected, as higher roughness can limit the effective contact area, thus reducing the frictional forces [28, 29].

At higher loads (60 N), the static friction behavior appears to shift. The weaker correlation between surface roughness and static friction indicates that other factors, such as rubber hardness, become more influential. The negative correlation with Shore A hardness and indentation force at 60 N is consistent with Voigt et al.'s findings, which demonstrated that softer rubbers, despite their higher surface roughness, tend to compress more, leading to a higher contact area and, consequently, higher friction [18]. For dynamic friction (μ_k), the results indicate that surface roughness remains a dominant factor under both loading conditions. The positive

correlation with adhesion energy (E_{adh}) suggests that adhesion plays a significant role in dynamic conditions, where the contact mechanics are influenced by the rubber's ability to maintain adhesion during motion.

Whilst conventional elastomer tribology suggests that a smooth surface would exhibit a lower static friction coefficient due to the propagation of stress relieving Schallamach waves, the rough granite interface in this study is expected to disrupt their propagation [27, 30]. It is evident that the contact dynamics are instead dominated by compliance and adhesion of the rubber to the rock interface, which for smoother rubbers giving a larger contact area within which friction is increased for surfaces exhibiting higher surface adhesion. This study reinforces the notion that the performance of climbing shoe rubber under various conditions is a complex interplay of multiple factors, including contact topography, material hardness, and adhesion.

A key finding of this study is that the smoother SMi6 and SC4 rubber surfaces consistently exhibit both high static friction coefficients and less drastic transitions between stick–slip behaviors (low slip factor), irrespective of their contrasting hardness values. Whilst this is partially owing to the improved contact compliance compared to the rougher XSG2, XSF, and XSE samples, this effect is compounded by the high adhesive energy for SMi6 and SC4 surfaces (SMi6, $E_{adh} = 52.7$ mJ and SC4, $E_{adh} = 72.8$ mJ) is an order of magnitude above the XSG2, XSF and XSE rubbers.

Voigt et al. [18] noted from their study that the softer, smoother rubber samples from their selection displayed a persistently higher static friction coefficient. A smooth and soft rubber sample was also shown to have 100-fold higher adhesion behavior to the other samples. Mohan et al. [27] found that 'slip-resistance' values of rubber shoe soles decreased when the material Shore-A hardness increased from 65 to 89. Soft rubbers were shown to have a greater effective contact area and more pronounced microscopic deformation when mechanically interlocking with the surface asperities of the counter-surface, hence an increase in slip resistance is observed. It was therefore concluded that a higher conformation with counter-surface asperities gave rise to a higher friction coefficient. There is an observed reduction in adhesion to the counter-surface with harder rubber compounds due to a higher resistance to indentation and topographical interlocking; therefore, a lower dynamic friction coefficient is observed [31–34].

In this study, the SMi6 compound exhibits the highest static and dynamic friction trends alongside the second highest surface adhesion, confirming its reputation among climbers for exceptional grip on polished surfaces, making it a preferred choice for competition climbers [4, 35]. Under low applied loads, static friction is dominated by the adhesive energy of the climbing shoe rubber interface, and therefore favors rubber surfaces that are smoother and more conformal to the counter-surface. Under higher applied loads, where the asperities of rubber surfaces are more deformed to achieve a high contact area, a higher degree of static friction is achieved by softer rubbers, with a reduced dependency on surface roughness. Under dynamic conditions, dynamic friction in both loading conditions is consistently enhanced by rubbers that provide a high adhesive energy and low surface roughness, which will mesh with the contact interface to increase friction [20]. The sensitivity of dynamic friction to rubber hardness is diminished at low loads. However, softer rubbers tend to exhibit increased dynamic friction under higher loads.

5.3 Material wear

Voigt et al. [18] found that the harder rubber materials were less sensitive to abrasive wear and damage. The rubbers that exhibited the highest and lowest material wear were the SMi6 and XSF rubbers respectively. Both rubbers exhibit comparatively low hardness values, with SMi6 being the softer of the two, which indicates that additional factors affect wear mechanisms under these circumstances. The surface roughness of the XSF rubber is higher than that of the SMi6 rubber. Therefore, the more prominent asperities on the XSF surface may have a greater capacity for deformation in response to stresses without fracture than the less prominent asperities on the SMi6 surface [17]. The SMi6 rubber was shown to be the most adhesive of the collection, in addition to exhibiting the highest static and dynamic friction coefficients under both loading scenarios, whereas the XSF rubber had the second lowest adhesion values which would help contribute to its low wear properties. This implies that greater adhesive forces within the granite-rubber contact led to a greater tendency for adhesive wear to occur. The softness of the SMi6 and its increased surface adhesion leads to the 'tacky and sticky' feeling described by wearers [4, 35–37]. Many climbers usually relate the softness of the SMi6 rubber to its low durability, a similar trend observed within this study [4, 35, 36]. Strong adhesion is also linked to its reduced lifespan and lower durability due to prominence of accelerated wear features.

Low surface wear was observed for the two hardest textured rubber compounds, XSG2 and XSE, with the original surface texturing from the unworn surface still being visible. Surface texturing has been shown to influence tribological performance [38]. The surface texturing for all given Vibram rubber samples was composed of parallel vertical lines. The XSE sample showed signs of a hexagonal pattern superimposed onto its existing unidirectional scoring, studies [18, 39] have shown that this type of surface texturing led to the reduction of stick–slip behavior and may explain the observed reduction in respective friction coefficients.

6 Future work

A limitation of this study is the assumption made regarding the contact pressures and areas involved in climbing. The estimations of nominal shoe area and corresponding contact pressures are not based on empirical data from existing literature, as there is currently a lack of studies investigating the realistic biomechanics and contact mechanics of climbing shoe–rock interfaces. Consequently, the normal loads and contact pressures used in this study are simplified approximations. Future research should focus on developing a detailed biomechanical and contact model of the climbing shoe–rock interaction to provide more accurate estimations of contact forces, areas, and the conditions under which slip may occur. These insights could then be used to refine benchtop tribometer studies, making them more representative of real-world climbing scenarios.

This study serves as an initial yet valuable and novel investigation into the tribological properties of climbing shoe rubbers. Future work will focus on conducting more robust statistical analyses and expanding the dataset to include rubber compounds. By leveraging the mechanical and tribological testing methods, we aim to evaluate the differences and relationships between samples. This approach will provide deeper insights into the factors influencing friction and wear performance. Ultimately, this expanded research will build upon the preliminary findings presented here, enhancing our understanding, and leading to improved reproducibility and reliability in the assessment of climbing shoe rubbers.

7 Conclusions

This study investigated the tribological properties of climbing shoe rubbers, focusing on the relationship between material hardness, surface roughness, adhesive energy, and frictional characteristics. Findings reveal that climbing rubber performance is primarily influenced by the material's adhesion properties and the surface finish's roughness. Ball indentation tests showed that surface roughness and asperity deformation significantly affect indentation energy and force. Notably, rubber adhesion was not linked to material hardness, suggesting that surface roughness and proprietary rubber composition have a predominant impact on adhesive energy. Sliding friction tests identified a critical stick–slip transition crucial for climber stability, with softer and smoother rubbers exhibiting extended stick phases, emphasizing the role of rubber softness and deformability in enhancing friction. Pearson and Spearman analysis demonstrated a notable negative correlation between static friction coefficient and surface roughness at lower loads, alongside a positive correlation with adhesive energy, highlighting the complex interactions among these factors in climbing shoe performance. Finally, wear analysis indicated that softer, more adhesive compounds such as SMi6 exhibited higher wear rates, whilst a low material hardness may also conversely lead to reduced wear when combined with high roughness and low adhesion as observed with the XSF compound. Surface texturing is therefore shown to improve wear resistance at the expense of friction behavior. This novel pilot study aims to contribute to the development of tribological characterization methods for climbing shoe rubbers, with plans for future studies to examine a larger group of rubbers from more manufacturers, ultimately contributing to standardized reporting of climbing shoe rubber performance.

Data availability The data that support the findings of this study are available from the corresponding author upon reasonable request.

Declarations

Conflict of interest All authors have no conflict of interest to declare.

References

1. McHenry R et al (2015) Footwear in rock climbing: current practice. Foot 25(3):152–158
2. Wada T, Nakamura Y, Okamoto N (2009) Rubber composition for shoe sole and rubber foam composition. Google Patents
3. Vibram, repair catalog. Vibram
4. Angel (2023) The climbing shoe rubber comparison. https://www.climbingshoereview.com/about/
5. Blanchette MG, Powers CM (2015) The influence of footwear tread groove parameters on available friction. Appl Ergon 50:237–241
6. Arc K, Durand R, Di Domenico H. Higher shoe sole longitudinal bending stiffness improves speed-climbing performance. In: Congress book
7. Donahoe T, Luebben C (2014) Rock climbing: mastering basic skills. Mountaineers Books, Seattle
8. Leung J (2023) A guide to indoor rock climbing injuries. Curr Sports Med Rep 22(2):55–60

9. Sherman A, et al. (2023) Inhalation of climbing shoe particles is highly relevant for the human exposure to rubber-derived chemicals in indoor facilities
10. Dennis A (2019) Sustainable eco-friendly climbing shoes. https://blog.weighmyrack.com/sustainable-eco-friendly-rock-climbing-shoes/.
11. Burbach M (2004) Gym climbing: maximizing your indoor experience. The Mountaineers Books, Seattle
12. Tiwari A et al (2017) The effect of surface roughness and viscoelasticity on rubber adhesion. Soft Matter 13(19):3602–3621
13. ASTM International (2021) ASTM D2240–15 (2021) standard test method for rubber property—durometer hardness. ASTM, West Conshohocken
14. Efremov YM, Kotova S, Timashev P (2020) Viscoelasticity in simple indentation-cycle experiments: a computational study. Sci Rep 10(1):13302
15. Dorogin L et al (2017) Role of preload in adhesion of rough surfaces. Phys Rev Lett 118(23):238001
16. Mesarovic SD, Fleck NA (1987) Spherical indentation of elastic–plastic solids. Proc R Soc London Ser A Math Phys Eng Sci 1999(455):2707–2728
17. Persson BN (2006) Contact mechanics for randomly rough surfaces. Surf Sci Rep 61(4):201–227
18. Voigt D, Karguth A, Gorb S (2012) Shoe soles for the gripping robot: Searching for polymer-based materials maximising friction. Robot Auton Syst 60(8):1046–1055
19. Ciavarella M et al (2019) The role of adhesion in contact mechanics. J R Soc Interface 16(151):20180738
20. Afferrante L, Violano G, Dini D (2023) How does roughness kill adhesion? J Mech Phys Solids 181:105465
21. Berman AD, Ducker WA, Israelachvili JN (1996) Origin and characterization of different stick—slip friction mechanisms. Langmuir 12(19):4559–4563
22. Schallamach A (1971) How does rubber slide? Wear 17(4):301–312
23. Schallamach A (1963) A theory of dynamic rubber friction. Wear 6(5):375–382
24. Heinrich G, Klüppel M (2008) Rubber friction, tread deformation and tire traction. Wear 265(7–8):1052–1060
25. Scherge M, Gorb S (2001) Biological micro-and nanotribology. Springer Science and Business Media, Berlin, Heidelberg
26. Gorb S, Scherge M (2000) Biological microtribology: anisotropy in frictional forces of orthopteran attachment pads reflects the ultrastructure of a highly deformable material. Proc R Soc London Ser B Biol Sci 267(1449):1239–1244
27. Mohan R, Das BN, Sundaresan R (2015) Effect of hardness and surface roughness on slip resistance of rubber. J Test Eval 43(6):1574–1586
28. Lyashenko IA, Pohrt R (2020) Adhesion between rigid indenter and soft rubber layer: Influence of roughness. Front Mech Eng 6:49
29. Lorenz B et al (2013) Adhesion: role of bulk viscoelasticity and surface roughness. J Phys Condens Matter 25(22):225004
30. Arnolds S, Roberts A, Taylor A (1987) Rubber friction dependence on roughness and surface energy. J Nat Rubber Res 2:1–14
31. Derler S, Kausch F, Huber R (2008) Analysis of factors influencing the friction coefficients of shoe sole materials. Saf Sci 46(5):822–832
32. Kim I-J, Nagata H (2008) Research on slip resistance measurements—a new challenge. Ind Health 46(1):66–76
33. Fendley A, Medoff H (1996) Required coefficient of friction versus top-piece/outsole hardness and walking speed: significance of correlations. J Forensic Sci 41(5):763–769
34. Tsai Y-J, Powers CM (2009) Increased shoe sole hardness results in compensatory changes in the utilized coefficient of friction during walking. Gait Posture 30(3):303–306
35. Leonard L (2024) The best climbing shoe rubber. https://perfectclimbing.com/the-best-climbing-shoe-rubber/.
36. Walker N (2019) What's the best rubber for your rock shoes? Gripped: The Climbing Magazine, Toronto
37. Lemonick S (2021) The Science of Sticky Rubber. https://www.climbing.com/gear/the-science-of-climbing-shoe-sticky-rubber/.
38. Kato T et al (2012) Low friction seal for muddy water with textured surface. SAE Int J Passeng Cars Mech Syst 5:639–646
39. Gorb SN et al (2007) Insects did it first: a micropatterned adhesive tape for robotic applications. Bioinspir Biomim 2(4):S117